JOURNAL OF GUIDANCE, CONTROL, AND DYNAMICS
Vol. 23, No. 2, March–April 2000

Design and Piloted Simulation of a Robust Integrated Flight and Propulsion Controller

Declan G. Bates,* Sarah L. Gatley,† and Ian Postlethwaite‡
University of Leicester, Leicester, England LE1 7RH, United Kingdom
and
Andrew J. Berry§
Defence and Evaluation Research Agency, Bedford, England MK41 6AE, United Kingdom

A robust integrated flight and propulsion controller is designed for an experimental short takeoff and vertical landing aircraft configuration, using the method of $\mathcal{H}^\infty$ loop-shaping. The aircraft model used in the study is based on the Harrier airframe with the Pegasus engine replaced by a thermodynamic simulation of a Rolls-Royce Spey power plant, to allow the incorporation of advanced engine control concepts. The controller follows a two-inceptor strategy to command flight-path angle rate and velocity along the flight path, while simultaneously keeping several airframe and engine variables within specified safety limits. The centralized integrated flight and propulsion control system is evaluated in piloted simulation trials. Results indicate that level 1 or 2 flying qualities are achieved over the low-speed powered lift region of the flight envelope.

Nomenclature

e	= error signals
$G(s)$	= plant transfer function matrix
$K(s)$	= $\mathcal{H}^\infty$ loop-shaping controller
SPLIT	= engine thrust split, 0–1 dimensionless
u	= control inputs
Vt	= velocity along the flight path, kn
z	= controlled variables
α	= aircraft angle of incidence, deg
γ	= flight-path angle, deg
$\dot{\gamma}$	= flight-path angle rate, deg/s
η	= elevator position, −15 to +15 deg
η_RCS	= pitch reaction control system position, −15 to +15 deg
θ	= pitch angle, deg
$\bar{\sigma}$	= maximum singular value

I. Introduction

THE development of systematic methods for the integration of flight and propulsion controls over the low-speed, powered-lift flight envelope is a key technical requirement for current and future short takeoff and vertical landing (STOVL) aircraft.[1] Successful application of integrated flight and propulsion control (IFPC) technologies offers the potential to achieve significantly improved flying qualities, while simultaneously prohibiting violation of operational constraints dictated by engine safety considerations.

This paper presents results from the second phase of a program of research carried out at Leicester University, in collaboration with the Defence and Evaluation Research Agency (DERA), on the design of IFPC systems using $\mathcal{H}^\infty$ robust control techniques. Results from phase one of the program, on IFPC design for the VAAC (vectored thrust aircraft advanced flight control) Harrier aircraft, are given in Refs. 2–4. For the second phase of the study, a new simulation model of an experimental STOVL aircraft configuration was developed at DERA Bedford to investigate the incorporation of more advanced engine control strategies within an IFPC framework. Preliminary results from this phase of the program are presented in Refs. 5 and 6. This paper presents details of the full IFPC design process for an experimental STOVL aircraft, from formulation of system performance specifications to piloted simulation trials.

The paper is organized as follows. Section II describes the STOVL aircraft model produced for this study at DERA Bedford. Section III outlines the performance requirements for the IFPC system. In Sec. IV, the design of a centralized IFPC system using the technique of $\mathcal{H}^\infty$ loop-shaping is described. Sections V and VI discuss the setup of the piloted simulation trials and the corresponding controller evaluation results. Finally, Sec. VII offers some conclusions.

II. DERA Bedford Spey–Wem Simulation Model

The aircraft simulation model used in this study has been developed at DERA Bedford in order to investigate the problems and opportunities associated with the integration of flight and propulsion control systems for STOVL aircraft. The airframe model used in the simulation is based on the nonlinear DERA Bedford Harrier T.Mk4 Wide Envelope Model (WEM). This model has been used extensively in the VAAC Harrier research program[7] and has been established through flight trials as being an accurate representation of the real aircraft. To fully explore the possibilities for advanced engine control under an IFPC system framework, the original Pegasus engine previously included in the WEM has been replaced with a high-fidelity thermodynamic model of the Rolls-Royce Spey engine, produced by DERA Pyestock. The Spey is a two-spool reheated turbofan engine with the same basic architecture, for the purposes of control, as the EJ200, which is used to power the Eurofighter.[8] As shown in Fig. 1, both the compressor and the turbine are split into low-pressure (LP) and high-pressure (HP) stages and are connected by concentric shafts that rotate at different speeds. Each combination of compressor, shaft, and turbine is called a spool.

The thermodynamic model of the Spey allows the control law designer full access to engine parameters such as inlet guide vane angle (IGVA), fuel flow rate, and exit nozzle area (ENOZA). The engine thrust is vectored through four nozzles similar to the standard Harrier. Total thrust and high-pressure bleed flow to the reaction control system (RCS) are scaled to match Pegasus performance, and no duct losses are modeled in the rotating nozzles. The effect of high-pressure bleed flow (to the RCS) on the engine operating point is modeled, and the effect of front/rear thrust split on engine performance is assumed to be negligible. To increase the design difficulty, the front pair of nozzles have been moved forward and downward to displace the center of thrust from the center of gravity and introduce thrust/pitching moment interactions. The thrust from front and rear nozzle pairs can also be modulated and vectored independently. Representative nonlinear actuation systems including both rate and magnitude limits have been placed on all control motivators. The

Received 5 April 1999; revision received 11 August 1999; accepted for publication 18 September 1999.

*Lecturer, Engineering Department. Member AIAA.
†Doctoral Candidate, Engineering Department.
‡Professor, Engineering Department. Member AIAA.
§Research Scientist, Flight Management and Control Department.

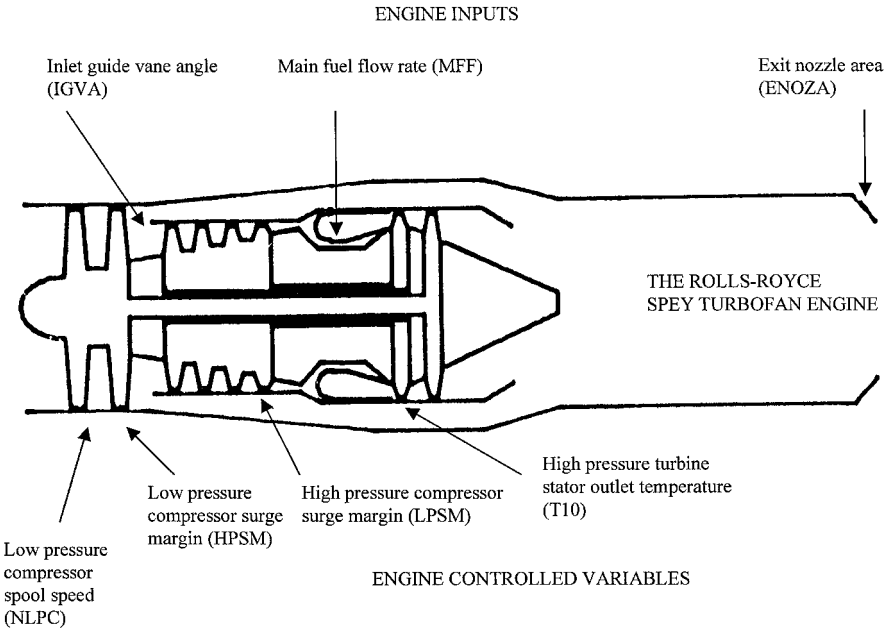

Fig. 1 Schematic of the Spey engine.

model offers a six-degree-of-freedom nonlinear simulation over a flight envelope from −20 to 250 kn. Linearized models for controller design purposes can be generated over the full flight envelope.

III. Control Law Requirements

The control law requirements for the Leicester University IFPC system design, detailed in Ref. 9, can be summarized as follows. The study focuses on the control of the longitudinal axis only. The pitch-axis controller follows a two-inceptor strategy. In this scheme fore/aft displacement of the center stick produces a change in flight-path angle rate $\dot{\gamma}$, and displacement of the left-hand inceptor demands aircraft velocity along this flight path Vt. Functional specifications for each inceptor are given as follows:

1) The first is the flight-path maneuver demand. The right-hand pitch control law will command $\dot{\gamma}$ and should actively hold flight path with the stick centered. Stick displacement will produce a flight-path rate demand up to a maximum of ±3 deg/s. Flight-path demands should aim to be decoupled from axial maneuvers, with a maximum of ±2 kn transient speed change during any flight path maneuvers between +30 and −20 deg.

2) The second is the flight-path velocity demand. Left-hand inceptor displacement will demand velocity parallel to the flight path Vt. Movement of the left-hand inceptor should obtain the fastest velocity magnitude response possible to arrest high descent rates in the hover and improve the handling qualities of the aircraft. Velocity demands should be decoupled from flight-path maneuvers for velocity changes of up to ±30 kn. A maximum transient of ±0.3 deg in flight-path angle is allowable during any velocity maneuver.

In a performance limited situation (e.g., maximum engine thrust is reached) the controller should prioritize satisfaction of flight-path demands over velocity demands. In addition to the preceding performance specifications, the following aircraft and engine limits are to be respected at all times:

1) Incidence boundary control is the first. To protect against extreme incidence angles, which can lead to lateral/directional instability, an incidence boundary of +12 to −6 deg is specified. In addition, maximum use of wing lift is desirable at all times to conserve fuel and engine life—the VAAC Harrier generally flies at a nominal angle of incidence of 6 deg during steady flight with transients within the preceding boundary acceptable during maneuvers.

2) Engine limits are the second. To protect engine components from dangerous overstress and overtemperature and to ensure avoidance of surge conditions, the following set of engine limits are to be respected during maneuvers, with priority being given to the first four variables (shown in Fig. 1): a) LP spool speed (NLPC) <102%, b) HP turbine stator outlet temperature (T10) <1430 K, c) HP compressor surge margin (HPSM) >10%, d) LP compressor surge margin (LPSM) >10%, e) HP spool speed <101%, f) HP compressor outlet temperature <810 K, g) combustion chamber pressure <2300 kPa, h) jet-pipe temperature <2200 K, and i) reheat fuel/gas ratio <0.055.

IV. Robust Centralized IFPC System Design

For the purposes of controller design, a linear representation of the Spey–WEM model (omitting lateral/directional airframe states) was generated at the 80-kn level flight trim point of the STOVL flight envelope. At this flight condition propulsion system generated forces and moments have largely taken over control from the aerodynamic effectors as the aircraft approaches the hover flight phase, and the aircraft is longitudinally unstable. The resulting state-space model of the integrated airframe and engine systems, plus actuators, has 35 states and is of the form

$$\dot{x} = Ax + Bu, \qquad y = Cx + Du$$

The control inputs are given by $u = [\eta, \eta\_RCS$, front nozzle position (FNOZ), rear nozzle position (RNOZ), SPLIT, main fuel flow (MFF), ENOZA, IGVA], whereas the vector of outputs y includes 8 airframe and 19 engine variables. Based on the performance requirements detailed in the preceding section, the vector of controlled variables z was chosen as $z = (\dot{\gamma}, Vt, \alpha$, NLPC, T10, HPSM, LPSM).

The angle of incidence α was included in z to explicitly minimize deviations from its trim point during maneuvers. In Ref. 9 the four engine variables NLPC, T10, HPSM, and LPSM were identified as having the most critical effect on the overall structural integrity of the engine and are thus included explicitly in z for the purposes of control.

The controller design procedure used in this study is based on $\mathcal{H}^\infty$ robust stabilization combined with classical loop shaping, as first proposed by McFarlane and Glover in Ref. 10. The resulting $\mathcal{H}^\infty$ loop-shaping design method is essentially a two-stage process. First, the open-loop plant is augmented by (generally diagonal) weighting matrices to give a desired shape to the singular values of the open-loop frequency response. Then, the resulting shaped plant is robustly stabilized with respect to coprime factor uncertainty using $\mathcal{H}^\infty$ optimization. A particular implementation structure[11] for $\mathcal{H}^\infty$ loop-shaping controllers is shown in Fig. 2. With reference to this figure, the weighting matrix $W_1(s)$ is chosen to add integral action and ensure reasonable roll-off rates for the open-loop singular values around the desired crossover frequencies. The scalar weighting

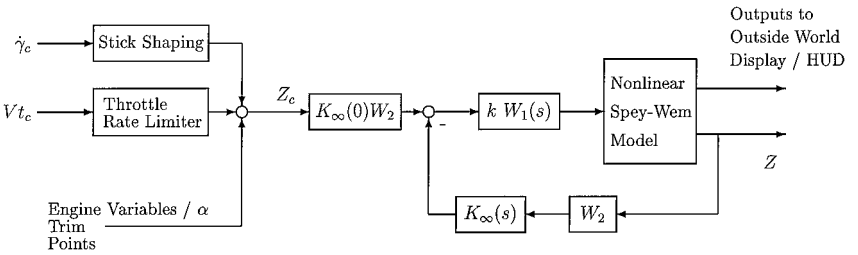

Fig. 2 Controller implementation structure for piloted simulation trial.

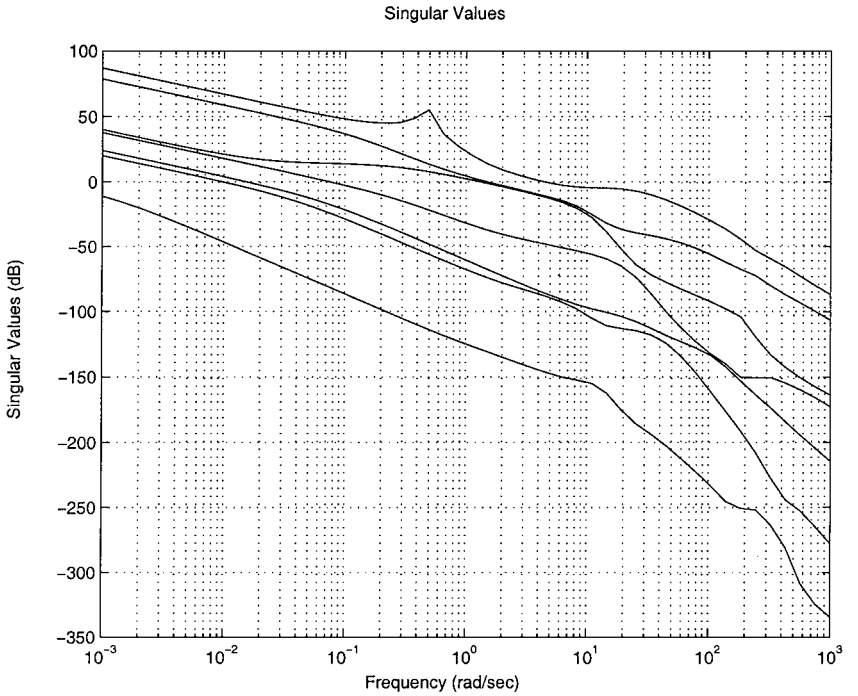

Fig. 3 Open-loop singular values after robust stabilization.

matrix k is then used to adjust control actuation requirements to respect the various effector rate and magnitude limits. In this configuration the nonlinear Spey–WEM aircraft model is assumed to be scaled so as to be approximately normalized with respect to maximum allowable input signals. The scalar matrix W_2 is used to prioritize airframe controlled variables (which must achieve specific handling qualities characteristics) over engine quantities (which have simply to be limited within certain values). This step is crucial to our integrated control strategy because the centralized controller must allow certain engine variables such as compressor temperatures and pressures to deviate from their nominal values during flight-path maneuvers. Tight control of all engine variables corresponds to demanding complete decoupling of these variables from large dynamic thrust changes. The resulting controllers would inevitably produce seriously degraded thrust response characteristics in nonlinear simulation caused by actuator saturation. The tradeoff between satisfaction of performance specifications and respecting limits on safety critical engine variables is thus explicitly built into the controller design process, via selection of the various weighting functions. For the controller discussed in this paper, the weighting matrices were chosen as

$$k = \text{diag}(.1, .1, .24, .24, .24, .2, .2, .2)$$

$$W_1 = [(s + 2)/s] \times I_{8\times 8}$$

$$W_2 = \text{diag}(1, 1, 1, 1/200, 1/800, 1/200, 1/500)$$

The second stage of the $\mathcal{H}^\infty$ loop-shaping design method involves the use of $\mathcal{H}^\infty$ optimization to robustly stabilize the shaped plant against a particular type of uncertainty description, based on stable perturbations to each of the factors in a coprime factorization of the plant. For a plant $G(s)$ with normalized left coprime factorization[12] $G = M^{-1}N$, a perturbed plant model can be written as

$$G_p = (M + \Delta_M)^{-1}(N + \Delta_N)$$

where Δ_M and Δ_N are stable unknown transfer functions that represent the uncertainty in the nominal plant model G. This arrangement removes the usual restriction included in other uncertainty models for the nominal and perturbed plants to have the same number of unstable poles. The objective of robust stabilization is then to compute a feedback controller that stabilizes the family of plants G_p. A bound for the size of the uncertainty in G_p can be defined as

$$\|[\Delta_N \Delta_M]\|_\infty \preceq \epsilon$$

where ϵ is then the stability margin. The optimal robust stabilization controller $K_\infty(s)$ is thus the controller that maximizes this stability margin for a given shaped plant. This controller can be computed explicitly by solving two Ricatti equations, thus avoiding the iterative procedures required in general $\mathcal{H}^\infty$ optimization. It has also be shown theoretically that for $\epsilon > 0.25$ 1) the original loop shapes are largely preserved, thus retaining the desired nominal performance,[10] and 2) the closed-loop system will have good robust performance properties.[11] For our design the controller $K_\infty(s)$ gave a value of ϵ equal to 0.252, thus guaranteeing closed-loop stability for coprime factor uncertainty of at least 25%. Finally, the constant prefilter $K_\infty(0)W_2$ is formed to ensure zero steady-state tracking error, assuming integral action in W_1. The order of the resulting $\mathcal{H}^\infty$ loop-shaping controller is then equal to the order of the shaped plant plus the weighting functions, i.e., 51 states. The open-loop singular values of the resulting system after robust stabilization ($W_1 G W_2 K_\infty$) are shown in Fig. 3. From the figure we

see that the singular value loop shapes correspond to the classical requirements for tracking performance and robustness—high gain at low frequencies and gentle roll off around crossover. Also, the achieved bandwidths correspond to the maximum rate limits for the various control effectors. Performance properties of the controller just described were initially examined via PC-based frequency domain and nonlinear time-domain simulations (see Ref. 6 for further details). The level of performance indicated by this analysis pointed to general satisfaction of the specifications set out in Sec. III, and thus subsequent formal evaluation of the IFPC system was conducted at DERA Bedford, as described in the following section.

V. Piloted Simulation Trial

Piloted simulation trials were conducted on DERA Bedford's Real Time All Vehicle Simulator (RTAVS). RTAVS is a fixed-base simulator with an immersive, backprojected, outside world display with a field of view of +135 deg/−45 deg vertically by ±135 deg horizontally. The aircraft simulation models are run on PCs with a networking facility that allows large models to be spread over several processors, or a series of aircraft models to be flown in separate cockpits in the same outside world environment, or both. The cockpit and instrumentation for this trial was representative of a generic fast jet. A dual linear throttle was used with the stick and rudder forces being simulated by springs. The head-up display (HUD) used for the trial is shown in Fig. 4. This display included a pitch attitude indicator, velocity vector diamond, thrust split and front, and rear nozzle angle indicators.

The Spey–WEM model and integrated control law were autocoded from the MATLAB®/Simulink[13] environment into C-code and then linked with the RTAVS code to provide executable software for the simulator. Stick shaping and a variable rate limit were added to the $\dot{\gamma}$ and the Vt demands, respectively. The $\dot{\gamma}$ demand limit was applied by scaling the maximum stick deflections to ±3 deg. The executable code calls the same FORTRAN modules (aerodynamics, engine, and RCS system) as the original Simulink diagram. Finally, the pilot inputs to the Spey–WEM model were mapped to the cockpit, and the aircraft states were mapped to drive the outside world view and the HUD.

The aim of the trial was to investigate the flying qualities and robustness of the integrated flight and propulsion controller for the Spey–WEM model. The simulator was piloted by three members of DERA Bedford's Flight Management and Control Department. Each of the pilots has extensive experience in the design and testing of advanced control laws for modern STOVL aircraft. To test the flying qualities of the IFPC system, a series of maneuver tasks were performed at and about the 80-kn design point, as described in the next section. The controller design specifications limited $\dot{\gamma}$ to ±3 deg/s for full fore and aft stick deflection, but gave no rate limit on Vt demands. A rate limit of 10 kn/s was implemented on the demand from the pilot's left-hand inceptor. This value was chosen as a compromise between providing adequate response to Vt demands while minimizing the coupling into γ and height. As the controller was designed for longitudinal motion only, the lateral and directional states of the model were fixed at zero. This allowed a direct evaluation of the longitudinal motion of the aircraft without the additional pilot workload involved in lateral/directional control.

VI. Discussion of Results

Pilot comments and ratings using the Cooper–Harper scale[14] for various demands on $\dot{\gamma}$ are shown in Table 1. Time histories of various aircraft states, engine variables, and actuators for 10-deg doublets on γ at both 60 and 100 kn (with Vt changing from 60 to 100 kn at $t = 80$ s.) are shown in Figs. 5–8. The $\dot{\gamma}$ demand signals from the stick were not recorded but consisted of demands corresponding to 10 or 20-deg doublets in all cases. The most common pilot comment for demands on $\dot{\gamma}$ was that at 60 or 80 kn the response was good but perhaps a little sluggish. At speeds of 100 kn or greater, the response became somewhat unpredictable. At all three speeds the coupling of $\dot{\gamma}$ demands into Vt was satisfactory, as pilots would generally not comment on Vt variations of less than 2 kn. At 80 kn the three pilots had no difficulty in acquiring desired flight-path angles, but the response was a little sluggish; this led to Cooper–Harper ratings

Table 1 Piloted simulation trial results for Gammadot demands

Pilot	Vt demand, kn	Gamma demands, deg	CHR	Pilot comments
1	80	±10	3	Slightly sluggish response
1	60	±10	3	Response more sluggish but better than at 100 kn
1	100	±10	4	Response less predictable
2	80	±10	3	Response is fine although a little sluggish
2	60	±10	3	Not a great deal of difference
2	100	±10	4	Gamma carries on after demand is over, leading to overshoot tendency
3	80	±10	2	——
3	60	±10	2	Less pilot compensation required than at 80 kn
3	100	±10	4	Little more difficult, more anticipation required and a little overshoot

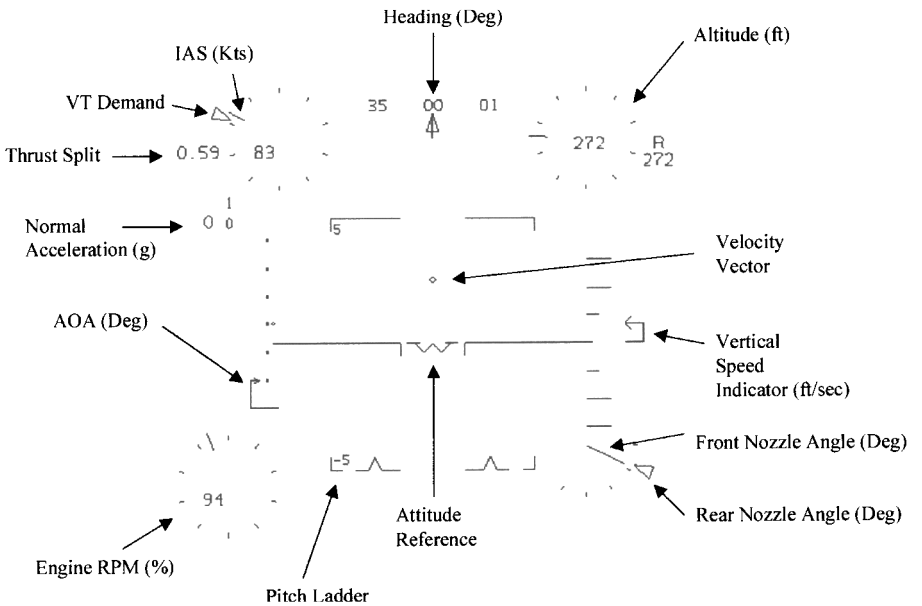

Fig. 4 HUD for the Spey–WEM simulation trial.

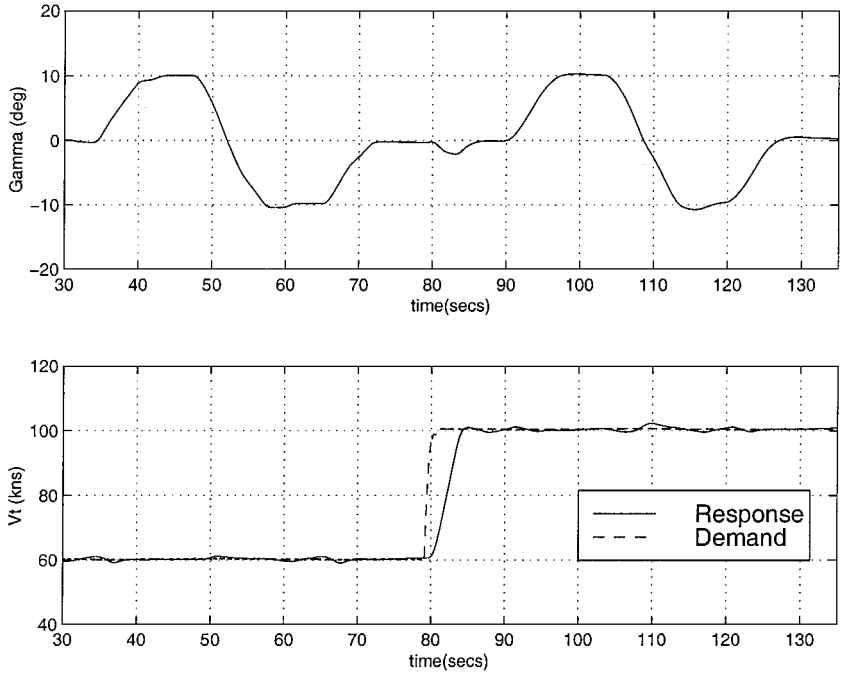

Fig. 5 $\dot{\gamma}$ demands at 60 and 100 kn.

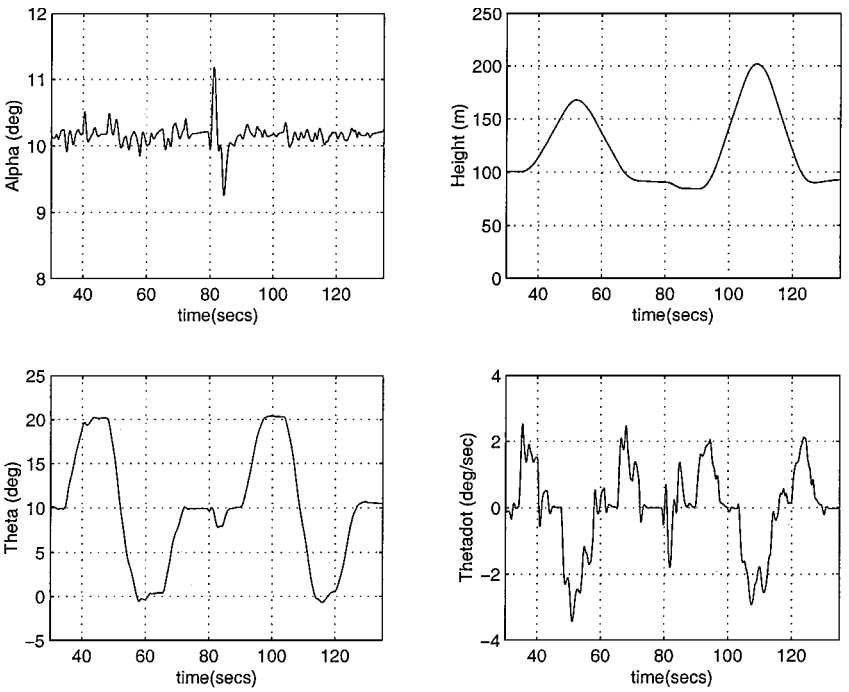

Fig. 6 Airframe variables, $\dot{\gamma}$ demands at 60 and 100 kn.

(CHRs) of 3, 3, and 2 for this task. Throughout the maneuver α was held to variations of approximately ±1 deg. Figure 7 shows the four internal engine variables that were controlled explicitly within hard limits. The limit for each variable is shown in each figure as a dashed line. NLPC and the LP and HP surge margins are all maintained within their respective limits. However, T10 transiently exceeds its maximum allowable value during the gamma maneuver at 100 kn. At this flight condition the CHR rating from each pilot shifted from level 1 to level 2, demonstrating that the achieved performance required some improvement. The different robustness characteristics of the controller for speeds below and above the design point arises from the change in control effectiveness of the front and rear nozzles as the aircraft accelerates from jet-borne toward wing-borne flight. These results indicate the need for controller scheduling at higher speeds to retain desired handling qualities over the full flight envelope.

Pilot comments and CHRs for demands on Vt are shown in Table 2. Time histories of aircraft states, engine variables, and actuators for 10 and 20 kn doublets on Vt are shown in Figs. 9–12. The general view of the pilots was that the response to Vt demands was excellent, but the resulting coupling into γ and altitude was too large. This coupling became worse for larger Vt steps as the aircraft moved away from the 80-kn controller design point. For both 10- and 20-kn doublets pilot 1 commented on the sharpness of the Vt response and tracking. Comments of "no compensation required" and "nothing to do but set throttle" led to a CHR of 1 for both tasks. However, the pilot did comment that these ratings did not really consider the γ interactions. Pilots 2 and 3 both noted the

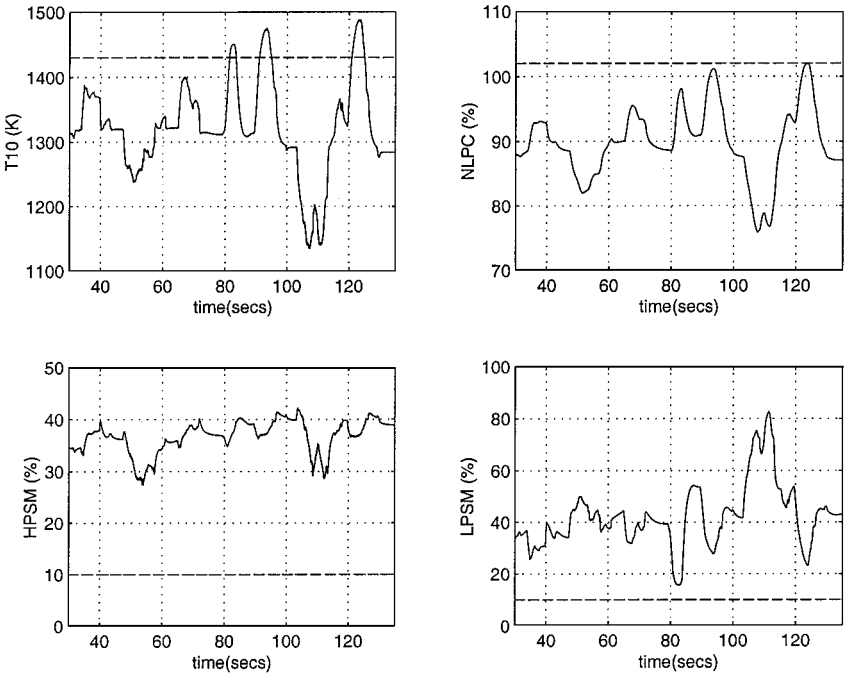

Fig. 7 Engine variables, γ demands at 60 and 100 kn .

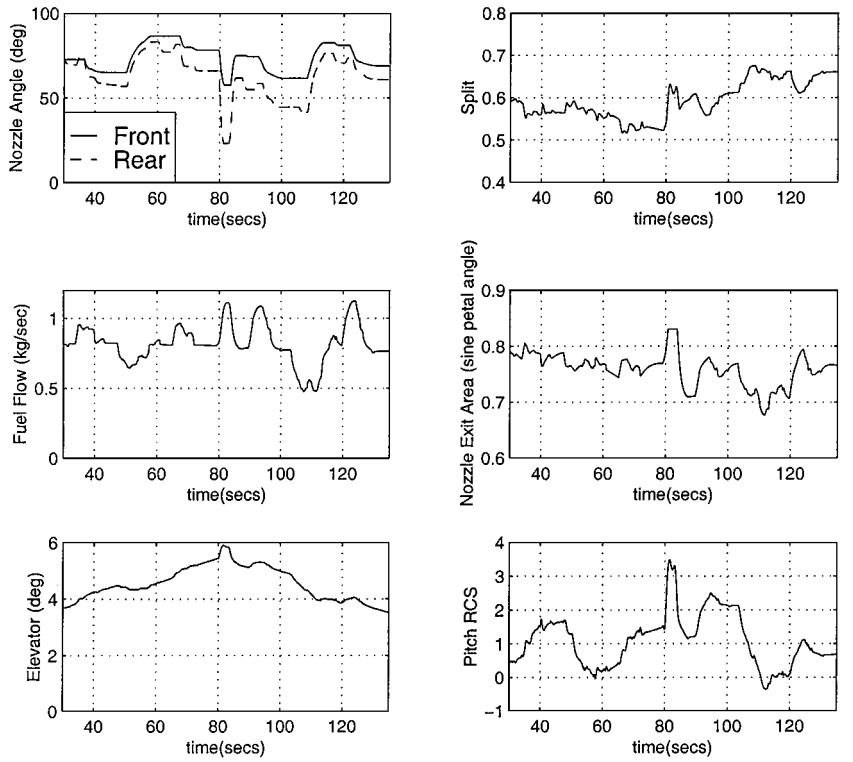

Fig. 8 Actuators, γ demands at 60 and 100 kn.

good speed control but also considered the γ interactions when giving their ratings. This led to CHRs of 2 and 3 for 10-kn demands and CHRs of 3 and 4 for 20-kn demands. The poorer ratings were a result of the coupling of Vt demands into γ and therefore height. Both pilots 2 and 3 also noted a slight overshoot in Vt. Figure 9 shows that the Vt response appears to have a time delay of around 0.8 s. Examination of the actuator time histories showed that this delay mostly resulted from the dead band (3 deg) of the nozzle actuators resulting in a 0.5-s delay in nozzle reaction to controller demands. Additionally, it was found that the size of the delay depends on the initial nozzle position. Figure 9 also shows the γ response to the Vt changes. There is significant coupling into γ with a maximum drop of greater than 1 deg for 10-kn demands and greater than 2 deg for 20-kn demands. Unexpectedly, this coupling into γ is negative for both positive and negative speed changes, leading to height reductions of approximately 4 and 8 m, respectively. Improvements in the level of γ interaction could be achieved by reducing the rate limit on Vt below its current value of 10 kn/s. Alternatively, future designs could control a blend of $\dot{\gamma}$ and γ, thereby explicitly controlling flight-path angle rather than just flight-path angle rate. Figure 10 also shows the α and θ response to the demands in Vt. The variations in α are larger than for the $\dot{\gamma}$ demand tasks but are still below the maximum incidence limit of 12 deg. The θ variation for the Vt demand was again greater than that caused by the $\dot{\gamma}$ demand,

Table 2 Piloted simulation trial results for *Vt* demands

Pilot	*Vt* demand, kn	Gamma demand, deg	CHR	Pilot comments
1	80 ± 10	0	1	Snappy *Vt* response
1	80 ± 20	0	1	Slight cross coupling with theta Nothing to do but set throttle Ratings didn't really consider the gamma interactions
2	80 ± 10	0	2	A little overshoot
2	80 ± 20	0	3	Coupling into gamma
3	80 ± 10	0	3	
3	80 ± 20	0	4	A little overshoot Increased coupling with gamma

but still small enough to be acceptable to the pilots. Figure 11 shows that for 10-kn demands on Vt none of the engine limits were exceeded, but the 20-kn doublet maneuvers caused the T10 limit to be broken.

To examine the effect of simultaneous demands on Vt and $\dot{\gamma}$, additional pilot tasks involving demands on $\dot{\gamma}$ during both steady climbing and steady descending flight were performed. These tasks were performed by only one pilot, and no CHRs were recorded. Comments from the pilot together with analysis of the trial data confirmed, however, that similar handling qualities were attained, with maximum coupling of Vt demands into γ of the order of 1.5 deg during both steady climbing and steady descending flight. Vt demands were tracked to a good level of accuracy, and the variation in α never exceeded 1 deg. Variations in θ were approximately 3 or

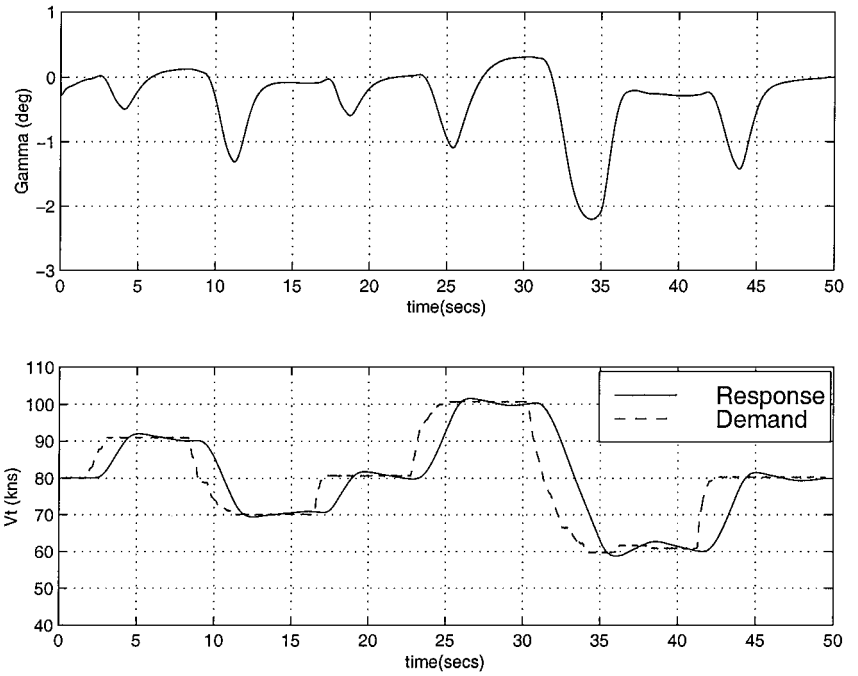

Fig. 9 10-kn and 20-kn demands on *Vt*.

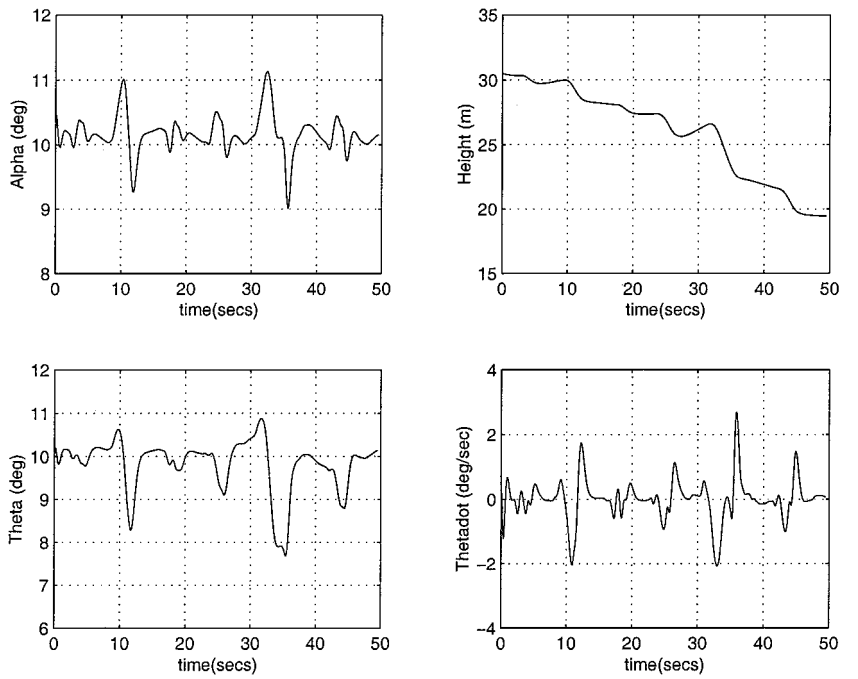

Fig. 10 Airframe variables, 10-kn and 20-kn demands on *Vt*.

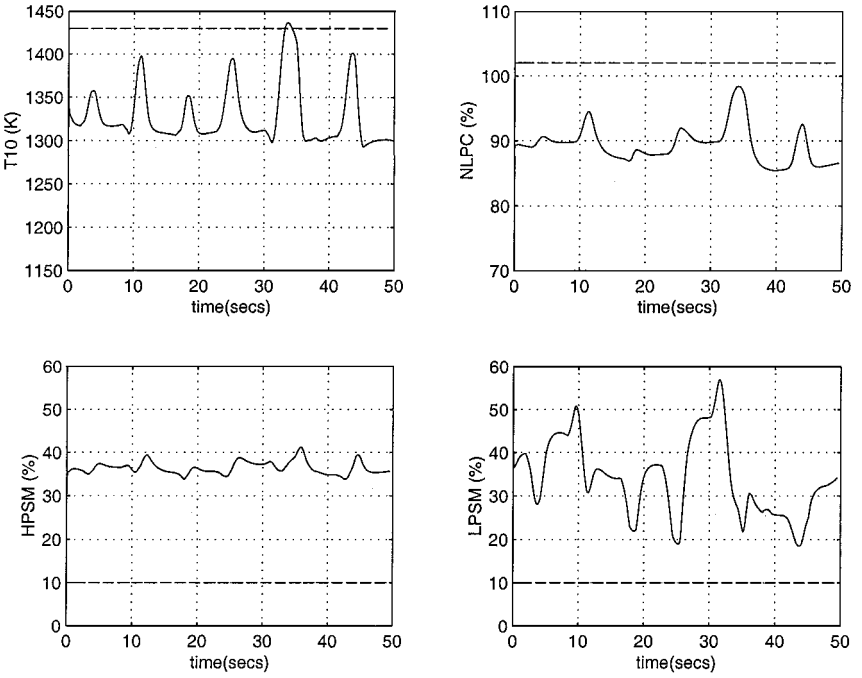

Fig. 11 Engine variables, 10-kn and 20-kn demands on *Vt*.

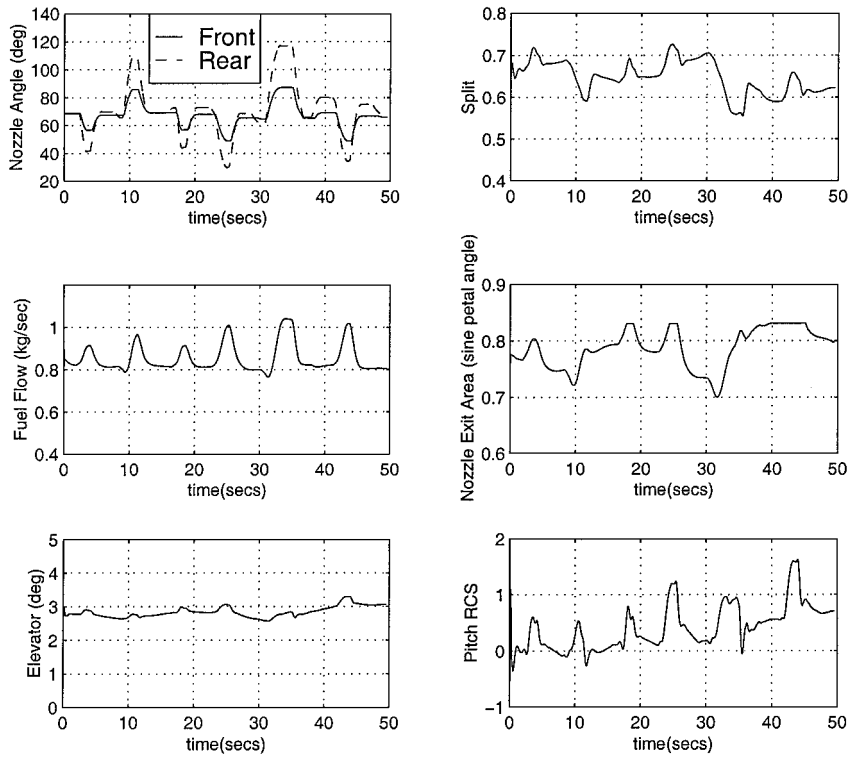

Fig. 12 Actuators, 10-kn and 20-kn demands on *Vt*.

4 deg during 20-kn velocity changes. However, both the T10 and NLPC engine limits were exceeded for 20-kn steps during climbing flight. The 20-kn task during descending flight also exceeded the T10 limit but to a lesser extent, and the other limits were preserved. The final task performed was simultaneous demands on $\dot{\gamma}$ and Vt. The controller tended to accelerate the aircraft toward the Vt demand before satisfying the $\dot{\gamma}$ demand. As flight path would normally be given priority over Vt, this indicates the need for an explicit method of prioritizing the demands on the controller.

During the course of the workup to the trial and during the trial itself, a problem with the FNOZ and RNOZ became evident. In the standard Harrier aircraft both front and rear nozzles are fixed at the same angle. However, for the current study the nozzle angles were allowed to vary independently. In general it was found that during a maneuver the front and rear nozzle angles would transiently vary independently and then return to the same value as another trim state was reached. However, after large demands in Vt or $\dot{\gamma}$, especially at higher than design speeds, the controller sometimes trimmed the aircraft with the nozzles at different angles. This can be seen in Fig. 8 where the front and rear nozzles come to rest approximately 5 deg apart. Once the nozzles had split in a steady flight regime, they tended to drift further apart over time with the result that they began to oppose each other. Although this effect was noted more often after Vt or $\dot{\gamma}$ tasks at higher than design speeds, it also occasionally occurred at the 80-kn design point after attempting to level out or descend after a steep climb. This demonstrated that the nozzle angle

drift is not merely a robustness issue. The cause of this behavior is the subject of current investigation by the authors.

The design choice of limiting the values of the engine parameters T10, NLPC, HPSM, and LPSM by including them as controlled variables proved to be quite successful at both the 80-kn design speed and at 60 kn. The variable T10 was seen to occasionally exceed its limit at 80 kn, but this could probably be addressed by tightening its control via adjustment of the $\mathcal{H}^\infty$ weighting functions. The additional engine variables detailed in Sec. III, which were not controlled directly, also generally stayed within their respective limits. However, at speeds of 100 kn or greater the strategy was less successful, with some variables transiently breaking their limits during maneuvers. This indicates the need for an additional nonlinear control scheme to guarantee hard limits, for example, by using a multimode switching strategy as in Ref. 15. For implementation purposes IFPC systems also generally need to be partitioned into lower-order subcontrollers, as discussed in Refs. 14 and 16. The development of general partitioning methods for centralized $\mathcal{H}^\infty$ loop-shaping controllers is the subject of current research by the authors.

VII. Conclusions

An integrated flight and propulsion control system was developed for a STOVL aircraft concept, based on the WEM model of the Harrier airframe with a Rolls–Royce Spey engine power plant. The IFPC system was designed using the method of $\mathcal{H}^\infty$ loop-shaping and was required to fully integrate the aircraft airframe and engine subsystems by 1) making optimal use of various propulsion system effectors for aircraft maneuvering control and 2) taking account of limits on safety critical engine variables as part of the overall two-inceptor control strategy. Robustness and handling qualities characteristics of the IFPC system were evaluated in piloted simulation trials. Level 1 flying qualities were attained for maneuvers in Vt and $\dot{\gamma}$ at the 80-kn design speed. Controller robustness and performance at lower speeds was good with no change in the CHRs. At speeds of 100 kn or greater, the $\dot{\gamma}$ response became less predictable, and the CHRs were typically increased to give level 2 flying qualities, indicating the need for a suitable scheduling strategy to retain desired handling qualities over the full flight envelope.

Acknowledgment

This work was conducted with the support of the U.K. Defence and Evaluation Research Agency through Extramural Research Agreement ASF/3819.

References

[1]Garg, S., "Robust Integrated Flight/Propulsion Control Design for a STOVL Aircraft Using $\mathcal{H}^\infty$ Control Design Techniques," *Automatica*, Vol. 29, No. 1, 1993, pp. 129–145.

[2]Postlethwaite, I., and Bates, D. G., "Integrated Flight and Propulsion Control System Design via $\mathcal{H}^\infty$ Loop-Shaping and Partitioning," *Proceedings of the AIAA Conference on Guidance, Navigation, and Control*, Vol. 2, AIAA, Reston, VA, 1998, pp. 989–998.

[3]Postlethwaite, I., and Bates, D. G., "Robust Integrated Flight and Propulsion Control System Design for the Harrier STOVL Aircraft," *Proceedings of the IEE International Conference on Control*, Vol. 2, Inst. of Electrical Engineers, London, 1998, pp. 1516–1521.

[4]Postlethwaite, I., and Bates, D. G., "Robust Integrated Flight and Propulsion Controller for the Harrier STOVL Aircraft," *Journal of Guidance, Control, and Dynamics*, Vol. 22, No. 2 1999, pp. 286–290.

[5]Bates, D. G., Gatley, S. L., Postlethwaite, I., Gillett, L., and Littleboy, D., "Robust Integrated Flight and Propulsion Control of an Experimental STOVL Aircraft," *Proceedings of the 37th IEEE Conference on Decision and Control*, Vol. 4, Inst. of Electrical and Electronics Engineers, 1998, pp. 4220, 4221.

[6]Bates, D. G., Gatley, S. L., Postlethwaite, I., and Berry, A. J., "Integrated Flight and Propulsion Control System Design Using $\mathcal{H}^\infty$ Loop-Shaping Techniques," *Proceedings of the 38th IEEE Conference on Decision and Control* (to be published).

[7]Tischler, M. B. (ed.), *Advances in Aircraft Flight Control*, Taylor and Francis, London, 1996, Chap. 6, pp. 159–186.

[8]Dadd, G. J., Sutton, A. E., and Greig, A. W. M., "Multivariable Control of Military Engines," *Proceedings of AGARD Conference No. 572—Advanced Aero-Engine Concepts and Controls*, AGARD, 1996, pp. 1–12.

[9]Berry, A. J., "Leicester University IFPC Control Law Requirements Document," DERA TM, Bedford, UK, unpublished, May 1998.

[10]McFarlane, D., and Glover, K., "A Loop Shaping Design Procedure Using $\mathcal{H}^\infty$ Synthesis," *IEEE Transactions on Automatic Control*, Vol. 37, No. 6, 1992, pp. 759–769.

[11]Hyde, R. A., *$\mathcal{H}^\infty$ Aerospace Control Design—A VSTOL Flight Application*, Springer–Verlag, London, 1995, pp. 191–199.

[12]Skogestad, S., and Postlethwaite, I., *Multivariable Feedback Control*, Wiley, New York, 1996, pp. 116–118.

[13]"Simulink: Dynamic Simulation for MATLAB," User's Manual, MathWorks, Natick, MA, 1997.

[14]Cooper, G. E., and Harper, R. P., Jr., "The Use of Pilot Rating in the Evaluation of Aircraft Handling Qualities," NASA TN D-5153, April 1969.

[15]Postlethwaite, I., Samar, R., Choi, B. W., and Gu, D. W., "A Digital Multi-Mode $\mathcal{H}^\infty$ Controller for the Spey Turbofan Engine," *Proceedings of the 3rd European Control Conference*, Vol. 4, European Union Control Association, Rome, 1995, pp. 3881–3886.

[16]Garg, S., "Partitioning of Centralised Integrated Flight/Propulsion Control Design for Decentralised Implementation," *IEEE Transactions on Control Systems Technology*, Vol. AC-1, No. 2, 1993, pp. 93–100.